On a New Approach for Instantaneous Rain Area Delineation in the Midlatitudes Using GOES Data

A. A. TSONIS AND G. A. ISAAC

Reprinted from JOURNAL OF CLIMATE AND APPLIED METEOROLOGY, Vol. 24, No. 11, November 1985
American Meteorological Society

Reprinted from JOURNAL OF CLIMATE AND APPLIED METEOROLOGY, Vol. 24, No. 11, November 1985
American Meteorological Society

On a New Approach for Instantaneous Rain Area Delineation in the Midlatitudes Using GOES Data

A. A. TSONIS AND G. A. ISAAC

On a New Approach for Instantaneous Rain Area Delineation in the Midlatitudes Using GOES Data

A. A. TSONIS* AND G. A. ISAAC

Atmospheric Environment Service, 4905 Dufferin Street, Downsview, Ontario, Canada, M3H 5T4

(Manuscript received 30 November 1984, in final form 8 May 1985)

ABSTRACT

Using satellite and weather radar data, a simple clustering analysis has been used in order to differentiate between raining and nonraining clouds. Based on these results, a scheme is proposed for instantaneous rain area delineation in the midlatitudes. Delineation of the rain areas will not require coextensive radar data which are only used to develop and evaluate the method. Warm season data during daylight hours were used to test the scheme. Results indicate that the proposed scheme has very good skills in delineating rain areas in the midlatitudes, resulting in an average probability of detection of about 66% and an average false alarm ratio of about 37%.

1. Introduction

Much of the analysis of the Geostationary Operational Environmental Satellite (GOES) visible and infrared images has concentrated upon rainfall estimation. A comprehensive review of satellite rainfall estimation methods to date was gathered by Barrett and Martin (1981). It summarizes, among others, the pioneering work of Barrett (1970), Woodley and Sancho (1971), Martin and Suomi (1972), Sikdar (1972), Follansbee (1973) and Gruber (1973) and the latest developments by Scofield and Oliver (1977), Griffith *et al.* (1978), Stout *et al.* (1979) and Lovejoy and Austin (1979).

Scofield and Oliver (1977) introduced a sophisticated decision-tree method which enables a meteorologist to estimate point rainfall rates on the basis of the two preceeding half-hour sets of GOES infrared data. With some skill, areas of more intense rain can be determined. Griffith *et al.* (1978), using a technique where a cloud area is defined by an infrared or visible threshold, were able to estimate rain amount from GOES imagery. They argued quite plausibly that the flux of rain (integrated rainfall over the raining area) from convective clouds can be determined from a life history of the area of convective cloud. In addition, Stout *et al.* (1979) proposed a method to estimate volumetric rainrates from the change of the cloud area in time. The cloud area was again defined by a visible or infrared threshold. The above methods, which are called life history methods, show good skills in mapping rainfall over an area for a specific time span (a season, for example) and in issuing flash flood warnings.

In a different approach, Lovejoy and Austin (1979) and Bellon *et al.* (1980) developed techniques which delineate instantaneous rain areas from coextensive radar and satellite (visible and infrared) data. These techniques, which are called bispectral methods, are based on the derivation of the probability of rain in the visible/infrared domain. For a specific area (over which coverage by a training radar is available), the probability of rain is derived by considering the bivariate frequency distributions in the visible/infrared domain of the raining and of the nonraining points. The derived probability of rain is then applied outside the area covered by the training radar. The success of the method outside the training area is usually evaluated by another radar (verifying radar). The above techniques show good skills in delineating the rain area over the range of the training radar but the accuracy decreases with distance outside that range (Pat King, personal communication, 1984). One explanation is that the bivariate frequency distribution, and therefore the derived probability of rain, are representative of the air mass over the radar covered area but they become less and less representative as the air mass changes with distance. In a real-time operation of such a scheme, weather radar information must be provided (Bellon *et al.*, 1980). Thus the above techniques are not easily applicable over remote areas where there is no radar coverage, or in cases where there are no echoes over the radar covered area.

The purpose of this paper is to describe a method which is a first step towards delineating instantaneous rain areas in the midlatitudes from the visible and infrared images *alone*. Radar data will be used as "ground truth" in developing and evaluating the method, but in a real-time operation the method can be applied without the need of coextensive weather radar data. It should be noted that the satellite delineated rain area

* Present affiliation: Dept. of Geological and Geophysical Sciences, University of Wisconsin-Milwaukee, Milwaukee, WI 53201.

in this paper, as well as in the references above, refers to areal extent of the rain aloft and not at the ground.

2. Data

The satellite data used in this work are GOES East visible (0.54–0.70 μm wavelength) and infrared (10.5–12.6 μm wavelength) images. The temporal resolution of the satellite data is 30 minutes and the spatial resolution is 4 × 4 km. It should be noted at this point that the true resolution of the sensed infrared images is 8 × 8 km. From these images, 4 × 4 km resolution images have been constructed for a better resolution equivalence between the infrared and visible data (Bellon, 1979). The intensity range of the visible image is 0–63 and that of the infrared is 0–255.

The visible count is taken to be an indication of cloud thickness while the infrared count refers to cloud or land temperature. The infrared count C_{IR} is an approximation to the temperature T of the emitting cloud or land by the conversion formula

$$T = 330\ \text{K} - \frac{C_{IR}}{2}, \quad \text{for} \quad C_{IR} \leq 176,$$

$$T = 418\ \text{K} - C_{IR}, \quad \text{for} \quad C_{IR} \geq 176.$$

The relation between visible count C_{VIS} and cloud thickness is more intricate and uncertain. The three-dimensional cloud structure, its composition and solar zenith angle are the main factors influencing the computed thickness. Normalization, taking into account the sun's elevation angle from the horizon (z), has been applied to the visible data. The normalization factor is simply taken equal to $1/\sin^{1/2}(z)$. More information on the normalization of the visible data can be found in Bellon *et al.* (1982). The data were tested for relative shifts between the visible and infrared images according to Tsonis (1984a). No such shifts were observed.

The analysis of the data was restricted to the area in Ontario, Canada, which is covered by the C-band Woodbridge weather radar (Crozier and Scott, 1981), indicated by the dark circle in Fig. 1. Table 1 gives a summary of the satellite and radar data used in this study. The training sample is used to develop the scheme and the verifying sample is used to test the success of the scheme. The third column indicates whether there was rain indicated by the radar during the corresponding hours (R for rain, N-R for no-rain) and what type (C for convective and N-C for nonconvective).

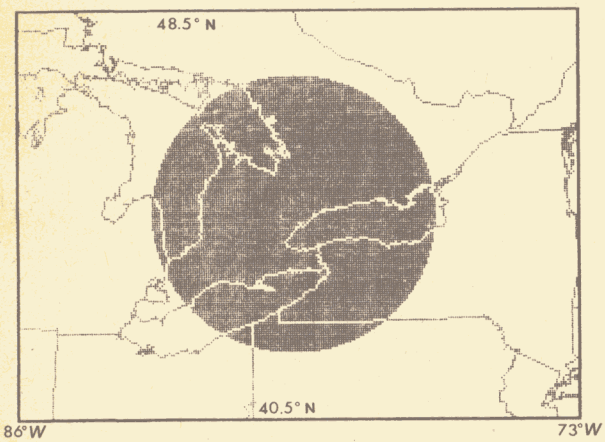

FIG. 1. The geographical area considered in this study. The satellite data analysis is restricted inside the dark circle which represents the area covered by the Woodbridge weather radar.

TABLE 1. Summary of the data used in this study.

Date	Period (GMT)	Radar results
	Training sample	
1 July 1982	1100–2230	*N-R*
10 July 1982	1200–2200	*N-R*
14 July 1982	1200–2300	*N-R*
27 July 1982	1230–1900	*R*(*N-C*)
28 July 1982	1400–2200	*R*(*C*)
3 August 1982	1200–2230	*N-R*
23 August 1982	1200–2300	*R*(*N-C*)
2 May 1983	1730	*R*(*C*)
20 May 1983	1200–1930	*N-R*
6 June 1983	1230–1730	*R*(*N-C*)
27 June 1983	1430–2200	*R*(*N-C, C*)
	Verifying sample	
4 July 1983	1230–2330	*R*(*C*)
29 July 1983	1330–2330	*R*(*N-C*)
21 July 1983	1730–2300	*R*(*C*)
13 May 1984	1330–1900	*R*(*N-C*)
15 May 1984	1430–2030	*N-R*
18 May 1984	1230–1930	*N-R*
23 May 1984	1300–2200	*R*(*N-C, C*)

3. Data analysis and methodology

The initial step taken in this work was to consider the GOES visible image over the radar covered area and then to produce series of maps, each map showing the cloud coverage for a different visible threshold. The same procedure was then repeated for the GOES infrared image. This was done in order to examine the ability of the satellite data to distinguish raining and nonraining clouds. Those maps were then compared with radar data. It was discovered that when the radar indicated precipitation, there was, almost always, a visible threshold which defined a cloud coverage very similar to the rain areas showing on the radar CAPPI (Constant Altitude Plan Position Indicator) maps and especially on the echo top maps. That visible threshold was not the same for every case. Such a conclusion was not obtained for the infrared images, except for some cases which will be discussed later.

The echo top maps show the maximum height above the ground of the observed radar echoes. Therefore, an echo top map will indicate the areal extent of the rain, independent of altitude. The echo top maps do not carry any rainfall rate information but they give a better indication of the actual areal extent of the rain over a

specific region, as compared to any level CAPPI or to any elevation angle PPI. They are particularly useful in drawing attention to precipitation not yet reaching the ground and to the common feature of overrunning ahead of an advancing warm front (Crozier and Scott, 1981). Since there is no reason for the satellite images to delineate rain areas at a specific altitude, it was decided to use the echo top maps as "ground truth" of the areal extent of the rain aloft. Note that radar echoes do not necessarily indicate rain. Echoes at higher levels sometimes may indicate snow or ice which will melt at lower levels falling at the ground as rain (if not evaporated). In this study liberty was taken to consider any radar echo as representing rain.

The use of the radar data at this point indicates whether or not the clouds over the radar-covered area are raining. However, the purpose of this paper is to present a method of delineating rain areas from the satellite images alone. This means that, in the absence of a radar, the differentiation between raining and nonraining clouds has to be achieved by some other way. The problem of rain area delineation using only satellite data at this point stands as follows: 1) differentiation between raining and nonraining clouds, and 2) definition of that specific visible threshold which will delineate the rain areas within the raining clouds. The differentiation between raining and nonraining clouds was achieved through the bivariate frequency distributions (or two-dimensional histograms) in the visible/infrared domain.

The use of the bivariate frequency distributions of visible and infrared data has been proven very useful in distinguishing rain areas with satellite data (e.g., Lovejoy and Austin, 1979 and Bellon *et al.*, 1980). In addition, Tsonis (1984b) used bivariate frequency distributions together with spatial characteristics in order to differentiate between various classes that exist in the satellite images. Tsonis concluded that the number of peaks in a frequency distribution is an indication of the number of classes that exhibit different spectral characteristics. The peaks in the distributions were attributed to three main classes, namely: clear skies/no snow cover, clear skies/snow cover, and clouds. Rain area or differentiation between raining or nonraining clouds was not attempted by Tsonis (1984b) and was not readily feasible mainly because winter data were used. However, using warmer season data, examination of the frequency distributions pointed out that the location of the peaks in the two-dimensional histograms may be an indication of whether or not those peaks correspond to clouds that rain. This observation was adapted and developed into a scheme for differentiation between raining and nonraining clouds which is outlined in Table 2 and Figs. 2 and 3.

Table 2 represents the bivariate frequency distribution over the radar covered area for 1600 GMT 6 June 1983 and it is derived by subdividing the data into intervals 4 units wide in the visible and every 16 units in the infrared; reasons for selecting these increments will be discussed later. The resulting peaks are indicated by the circles. The location of each peak is then adjusted by considering the weight of the eight neighboring frequencies. The adjusted position of the peaks in the visible/infrared domain as indicated by crosses are shown in Fig. 2. For example, the peak that corresponds to frequency 849 should be located (without adjustment) at visible count 13.5 (middle of the interval 12–15) and at infrared count 103.5 (middle of the interval 96–111). Taking into account the weight of the neighboring frequencies, that peak is then positioned in Fig. 2 at visible count of about 15 and at infrared count of about 104. Such a procedure elimi-

TABLE 2. Bivariate frequency distribution in the "visible/infrared" domain for 1600 GMT 6 June 1983.

	Visible count															
Infrared count	0–3	4–7	8–11	12–15	16–19	20–23	24–27	28–31	32–35	36–39	40–43	44–47	48–51	52–55	56–59	60–63
240–255	0	0	0	0	0	0	0	0	0	0	0	0	0	0	0	0
224–239	0	0	0	0	0	0	0	0	0	0	0	0	0	0	0	0
208–223	0	0	0	0	0	0	0	0	0	0	0	0	0	0	0	0
192–207	0	0	0	0	0	0	0	0	0	0	0	0	0	0	0	0
176–191	0	0	0	0	0	0	0	13	(94)	84	169	479	894	(3123)	143	0
160–175	0	0	0	0	0	0	4	56	33	8	15	31	29	584	224	0
144–159	0	0	0	0	2	3	8	17	11	16	17	41	106	497	212	0
128–143	0	0	0	0	0	10	11	30	46	47	66	96	237	352	20	0
112–127	0	0	0	0	48	13	23	(126)	50	32	45	105	45	23	0	0
96–111	0	0	0	(849)	353	112	72	104	44	12	18	5	1	0	0	0
80–95	0	0	0	0	5	68	8	7	1	2	0	0	1	0	0	0
64–79	0	0	0	0	0	0	0	0	0	0	0	0	0	0	0	0
48–63	0	0	0	0	0	0	0	0	0	0	0	0	0	0	0	0
32–47	0	0	0	0	0	0	0	0	0	0	0	0	0	0	0	0
16–31	0	0	0	0	0	0	0	0	0	0	0	0	0	0	0	0
0–15	0	0	0	0	0	0	0	0	0	0	0	0	0	0	0	0

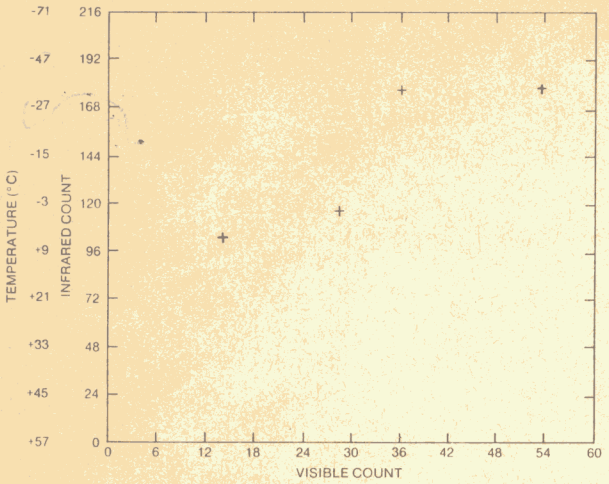

FIG. 2. Adjusted location of the peaks in Table 2 in the visible infrared domain. Case of 1600 GMT 6 June 1983.

nates, to a degree, the effect that the choice of the sampling intervals have upon the location of the peaks in a two-dimensional frequency histogram.

Since there is no snow on the ground, the peaks can be attributed only to clear skies/no snow cover (representing either land or water) or to clouds. Peaks that resulted from a clear skies scene can be easily identified either by visual inspection of the images or by their location in the two-dimensional histogram. As was demonstrated by Tsonis (1984b), peaks that represent a clear skies/no snow cover scene are always located at visible counts less than 27, with land giving higher responses than those of water. The remaining peaks are attributed to clouds and their division into raining or nonraining clouds was made as follows: the coordinates of each peak in Fig. 2 are defined by a peak's visible count (V_i) and by a peak's infrared count (I_i) where $i = 1, 2 \cdots n$ and n is the number of peaks. Each peak is then considered separately. Then a cloud area A_i defined by points with visible count greater than or equal to V_i and infrared count greater than or equal to I_i, is located within the radar-covered area. This can be effectively done by using color displays of the visible and infrared images. If the radar shows any rain within A_i, the peak is attributed to raining clouds. Otherwise, the peak is attributed to nonraining clouds. Although A_i may not be equal to the actual cloud area associated with the peak, it does represent most of the actual cloud area including the thicker and higher clouds within which rain is most likely to be found. After all peaks have been ascribed to raining or nonraining clouds, for presentation purposes, Fig. 2 changes to Fig. 3 where the peak that corresponds to clear skies/no snow cover (either land or water) is represented by a square, peaks that correspond to nonraining clouds are represented by circles and the peak that corresponds to raining clouds is represented by a triangle.

The procedure outlined in Table 2 and Figs. 2 and 3, for 1600 GMT 6 June 1983, is then applied to the other available data from the training sample. From each day, only data at least three hours apart are considered. In three hours, most of the air mass that exists at a given time over the radar covered area will have been replaced. The resulting peaks (which are representative of the air masses over that area) can be considered as independent. The final result (Fig. 4) is a two-dimensional scatter diagram of the responses of the various peaks that were generated from the training sample.

This two-dimensional feature space should then be partitioned in some fashion so that any other unknown points (due to peaks from another data set) are uniquely attributed to rain, nonraining clouds or clear skies. The most common procedures (known as clustering techniques) that are used to tackle this problem are the so-called supervised partitioning and the nonsupervised partitioning. In supervised partitioning, the method establishes classes with informational value and then checks whether those classes are separable. In nonsupervised partitioning, the reverse is true. The method establishes separable classes (or clusters) and then checks whether they have any informational value. For example, if supervised partitioning was used for the data in Fig. 4, classes with informational value such as clear skies, raining clouds and nonraining clouds should at first be established. These classes should then be checked to see if they are separable. On the other hand, if nonsupervised partitioning was used, separable clusters should be defined which then should be checked whether they can be attributed to classes with some informational value.

In Fig. 4 it is readily observed that clusters of points which correspond to nonraining clouds occur at two places: these clusters are centered at about visible count 30 and infrared count 104 and visible count 46 and

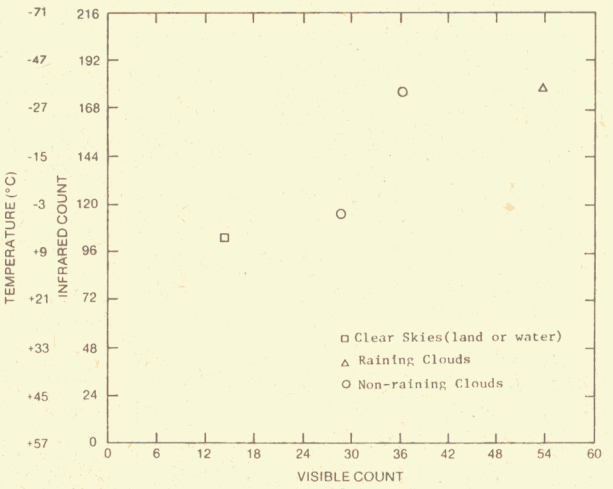

FIG. 3. As in Fig. 2 but showing the corresponding classes.

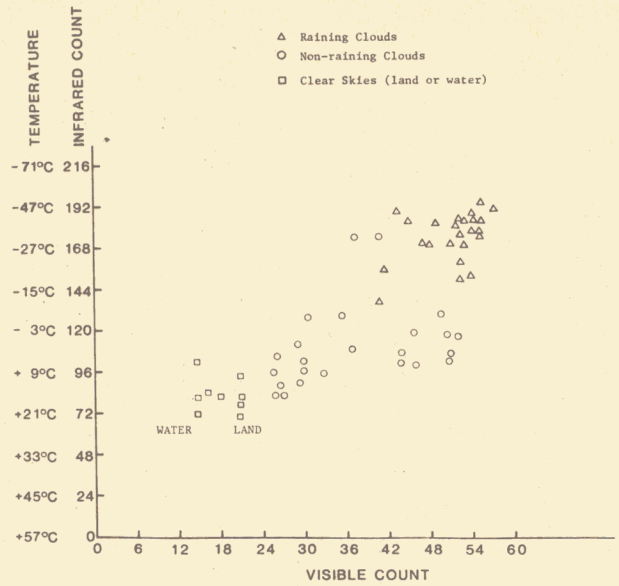

FIG. 4. Scatter diagram of the peaks generated from the training sample.

infrared count 110. This could be an indication that these clusters represent either two types of nonraining clouds which differ in informational value, or two different classes. In actuality, both conclusions are true. From the available satellite, radar and synoptic data, it was deduced that the nonraining clustering at higher visible and infrared counts consists of points which represent peaks that correspond to nonprecipitating low-level overcast (low-level stratus, stratocumulus, etc.), fog and haze. The other nonraining cluster consists of points which represent peaks generated from nonraining scattered or broken cloudiness (cumulus, altocumulus, cirrocumulus, cirrus, etc.). A new class (haze) has now been identified, which does not exhibit different spectral characteristics than that of a low-level overcast or fog. Fog is not considered a new class mainly because fog and low-level stratus are sometimes indistinguishable. The main purpose of this paper is the delineation of rain. The fact that fog and especially haze may be identifiable from the GOES visible and infrared data using similar techniques is an interesting problem but is beyond the scope of this work. However, based on this observation, further work on this topic has been performed and will be reported elsewhere. To summarize, it seems that a scatter diagram, produced from weather satellite data such as Fig. 4, may result in clusters which cannot be attributed to a specific class. In other words, some clusters may have more than one informational value. With respect to the problem in hand, any partitioning which will result in the differentiation between the peaks that represent raining clouds from the other peaks will be acceptable.

The partitioning procedure used in this paper is a blend of supervised and nonsupervised partitioning. According to that procedure, the points of Fig. 4 are divided into three major clusters as indicated in Fig. 5. These clusters have been defined subjectively but in such a way as to satisfy the following conditions: a) clusters are easily separable and b) all points that correpond to raining clouds are included in one cluster. Cluster 1 consists of points that are associated with clear skies (land and water) and with nonraining clouds (mainly broken or scattered clouds). Cluster 2 consists of points that correspond to nonraining low-level overcast, fog and haze. Cluster 3 consists of points assigned mainly to raining clouds. Two points in cluster 3 correspond to nonraining clouds. Having defined the three clusters, the conditional centroid or center point of each cluster is determined and is indicated by a cross. Next the locus of a point equidistant from these three centroids is plotted and results in three segments of straight lines as shown in Fig. 6. These straight lines form, in effect, decision boundaries (Lintz and Simonett, 1976), and every point in that space automatically becomes associated with the class (or classes) that correspond to each cluster. The dashed lines are explained later. As can be seen from Fig. 6, the points that correspond to peaks generated from raining clouds have been very effectively separated. There are two data points (indicated by arrows 1 and 2) in cluster 3 which are not associated with raining clouds. These points represent peaks that are associated with cirrus clouds. Interestingly, in both cases, there is an accompanying point at higher visible counts which is assigned to raining clouds (see Fig. 3). This is probably a reflection of the role of cirrus cloud as prodromes or as an exhaust product of storms.

Some other interesting features of Fig. 6 have been indicated by arrows 3, 4, 5 and 6. Arrows 3, 4 and 5

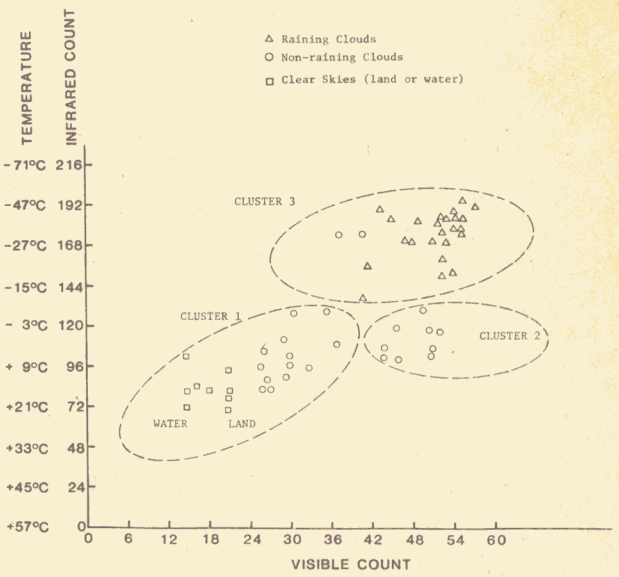

FIG. 5. Division of the peaks in Fig. 4 into three clusters (see text for details).

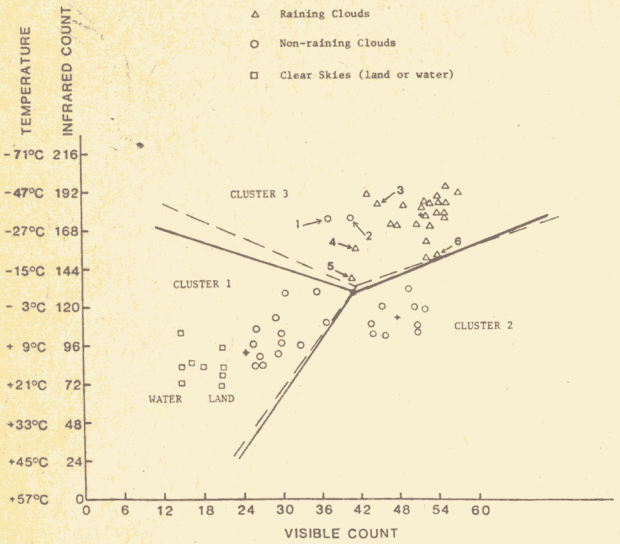

FIG. 6. Partitioning of Fig. 4 (or Fig. 5). The straight lines are the decision boundaries which separate the peaks that correspond to each cluster. The dashed lines are the corresponding decision boundaries when data from both training and verifying sample are considered.

depict (in chronological order) the sequence of 23 August 1982 when the corresponding precipitation area was constantly decaying with time. One can see the gradual motion of the peak away from the main clustering of the raining clouds and towards the "territory" of the nonraining clouds. The peak indicated by arrow 6 results from the images on 1830 GMT 27 June 1983 and corresponds to a steady widespread rain area. The other peaks, and especially those located at higher visible and infrared counts, have been generated from a mostly convective type of precipitation, even though a clear separation between the convective and the nonconvective cases is not evident. It may be that the location of a peak within the raining clouds' territory is indicative of the precipitation stage and/or intensity. Such a claim should be substantiated by further research dealing specifically with that question. It should also be mentioned that in partitioning Fig. 4 other approaches could be considered. For example, one could exclude the clear skies points from cluster 1 and work only with points that correspond to cloudy conditions. Such an approach will separate the raining points satisfactorily. However, by including the clear skies in cluster 1, a somewhat clearer separation of the raining points is achieved because the low visible and infrared value points of the clear skies weight this cluster towards the origin.

Figure 6 apparently depends on the climatology of the representative area. This means that the decision lines in Fig. 6 may not be the same over another area. Figure 6 should be produced for any area of interest. If radar coverage is not available, the attribution of the peaks to raining or nonraining clouds could be made by using ground synoptic station information or through the climatology of the area.

Three final points should be discussed. First, the dashed lines in Fig. 6. These lines are also decision boundaries generated using the training and the verifying sample together. This was done to test whether or not inclusion of another data set will influence significantly the location in the visible/infrared domain of the decision boundaries. Apparently, the changes are not significant and would not affect the proposed scheme. Second, from Fig. 6, one might conclude that rain occurs only from clouds with tops colder than -10 to -15°C. Figure 6 is a scatter diagram of the location of the peaks in the visible/infrared domain. Each peak that corresponds to raining clouds does not necessarily represent all the rain area. The rain area will include the points that correspond to the peak, as well as other points with lower infrared counts and therefore warmer temperatures. However, the fact that most of the rain points seem to be associated with cloud tops colder than -10°C may be an indication of the ice crystal process as the prevailing precipitation process over the area of investigation. Third, it was mentioned previously that peaks in the two-dimensional histograms resulting from sampling every 4 units in the visible and every 16 units in the infrared can be attributed to three main classes. As stated in Tsonis (1984b), choice of smaller sampling intervals will result in peaks which will belong to subclasses of the main classes. For example, peaks in the region of clouds will represent various types of clouds; peaks in the clear skies region will represent various types of ground coverage, soil types and so on. By increasing the interval, one is smoothing the histogram. The choice of the intervals depends on how much smoothing one desires so as to best meet the classification purposes. The purpose of this work was to delineate rain areas and not to identify different types of clouds. The choice of the above intervals is thus considered adequate.

4. The proposed scheme for instantaneous rain area delineation

A method has been developed to differentiate between raining and nonraining clouds. In order to delineate instantaneous rain areas, the determination of that specific visible threshold mentioned earlier must be determined. It should be emphasized that the decision boundaries derived in Fig. 6 refer to the peaks that represent the various classes and not to all points that are associated with a peak. Even though the peaks that correspond to raining clouds will be found in cluster 3 territory, the points that are associated with those clouds will not necessarily assume visible and infrared counts determined by the decision lines. The boundaries of Fig. 6 will differentiate between peaks that represent raining and nonraining clouds that would not necessarily yield the rain area.

The most satisfactory visible threshold which combined simplicity, objectivity and good results was found to be the visible count at which the peak that corresponds to raining clouds is located. In accordance with that concept, the following scheme was developed for rain area delineation over the area of investigation:

Step 1: Derive the frequency histogram in the visible/infrared domain and locate the peaks.

Step 2: Adjust the position of each peak by considering the weight of the neighboring frequencies and then position all peaks in Fig. 6.

Step 3:

a) If there are no peaks in cluster 3 territory, all points are assigned as no-rain.

b) If there is only one peak in cluster 3 territory located at visible count V_1 and no peak in cluster 2 territory, all points with $C_{VIS} \geq V_1$ are assigned as raining points.

c) If there is one peak in cluster 3 territory located at visible count V_1 and at infrared count I_1 and one peak in cluster 2 territory located at visible count V_2 and infrared count $I_2 (I_2 < I_1)$, an infrared threshold which will separate the points that belong to the two different peaks is determined. This infrared threshold (I_3) is defined as the infrared level whose distance (in counts) from I_1 and I_2 is directly proportional to the weight of the peaks expressed by their observed frequencies f_1 and f_2. Simple algebra yields that $I_3 = I_2 + [(I_1 - I_2) f_2/(f_1 + f_2)]$. All points with $C_{VIS} \geq V_1$ and $C_{IR} \geq I_3$ are then considered as raining points. If there is more than one peak in cluster 2 territory, then the above procedure is followed considering only the peak closest to I_1.

d) If there are two peaks in cluster 3 territory located at visible counts V_1 and V_2 (with $V_2 > V_1$) and no peak in cluster 2 territory, only the peak that corresponds to V_2 is considered and all points with $C_{VIS} \geq V_2$ are classified as raining points.

e) If there are two peaks in cluster 3 territory and one or more peaks in cluster 2 territory then steps 3d and 3c are followed in that order.

Early testing of the above scheme with the training sample revealed that, in some cases, too large a rain area was produced even though in most cases very satisfactory rain area delineation was achieved. This happened in cases of weakening rainfall and especially when the rain was about to end. Under such conditions (one of which is indicated by arrow 5 in Fig. 6) the rain area is much smaller than the cloud area. In situations like these, the failure of the scheme to produce a satisfactory rain area is due to the lack of a so-called "stability criterion." In Lovejoy and Austin (1979) the stability criterion was the restriction that the delineated rain area should be equal to that of the radar. In other words, their scheme stops delineating rain area when it has produced a rain area which is equal in size to that indicated by the radar. In this paper, the scheme has been designed to require no radar or any other rainfall data in delineating rain areas once Fig. 6 has been produced. Therefore, information on the extent of the rain will not be available and a stability criterion like the one in Lovejoy and Austin (1979) is not applicable. A suitable stability criterion was found as follows. For each point of Fig. 6 that corresponds to raining clouds, there exist a visible threshold V which according to the above scheme delineates the rain area. If one denotes the satellite delineated area by $\hat{A}_R$, and the radar indicated rain area by A_R, and plots $\hat{A}_R/A_R$ as a function of V, one gets Fig. 7. As can be seen from Fig. 7, the ratio of the two areas (the radar area is considered here as ground truth), is between 0.5 and 1.5 for approximately $45 \leq V \leq 57$. For $V \leq 45$, $\hat{A}_R/A_R$ takes much higher values. This indicates that the satellite derived rain area is much greater than the radar indicated area when the peak is located at visible counts less than 45. The above observation leads to the stability criterion where rain area delineation is restricted to points with $C_{VIS} \geq 45$, instead of $C_{VIS} \geq V$, when $V \leq 45$.

5. Evaluation

The evaluation of the rain area delineation techniques is usually based on the following variables:

N_N number of points correctly classified no-rain
N_R number of points incorrectly classified no-rain (misses)
R_N number of points incorrectly classified rain (false alarms)
R_R number of points correctly classified rain (hits).

Accordingly, the satellite delineated rain area can be expressed as:

$$\hat{A}_R = R_N + R_R.$$

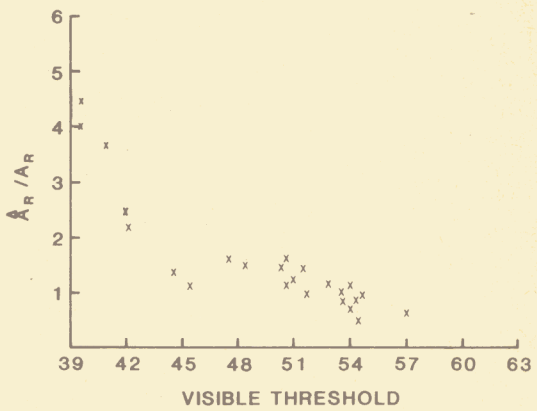

FIG. 7. The ratio of the satellite generated rain area to the radar indicated rain area as a function of the visible threshold; according to the scheme this delineates the rain area from the satellite images.

For the following formulations, A_R will denote the radar rain area as indicated by the radar echo top maps. From the above notation, many statistics have been devised in order to evaluate a rain area estimation method using satellite data. The most commonly used are:

1) The probability of detection (POD) defined as

$$\text{POD} = R_R/A_R;$$

2) The false alarm ratio (FAR) defined as

$$\text{FAR} = 1 - (R_R/\hat{A}_R);$$

3) The percent error f defined as

$$f = (N_R + R_N)/(R + N),$$

where

$$R = R_N + R_R,$$

$$N = N_N + N_R.$$

4) The areal bias β defined as

$$\beta = \frac{1}{n}\sum_n \hat{A}_R/A_R,$$

where n is the number of cases.

5) The error factor, ϵ_f, defined as

$$\epsilon_f = \frac{1}{n}\sum_n y$$

where

$$y = \hat{A}_R/A_R, \quad \text{if} \quad \hat{A}_R \geq A_R.$$

$$y = A_R/\hat{A}_R, \quad \text{if} \quad A_R > \hat{A}_R;$$

6) The root mean square error, ϵ_{rms}, defined as

$$\epsilon_{\text{rms}} = \overline{[(A_R - \hat{A}_R)]}^{1/2}/\bar{A}_R$$

where the bar indicates averages.[1]

A perfect method will give POD = 1, FAR = 0, f = 0, β = 1, ϵ = 1, and ϵ_{rms} = 0. However, none of these statistics can be considered as more representative of the success of the method than any other statistic. Each statistic gives additional information about the success of the rain area delineation from the satellite data. For example, the POD gives an idea of the ability of the scheme to "find" the rain. However, a scheme could create five or ten times larger rain area than the actual and still give a POD of one. Therefore, high POD should be accompanied by a small FAR in order to be meaningful. The percent error is representative of the error in rain area delineation with respect to the total area over which the method is applied. The percent error could be small even when POD is low and FAR is high, especially when we are dealing with small precipitation areas. The reverse could be the case as well. The areal bias and error factor give an idea as to whether or not the scheme systematically overestimates or underestimates the rain area and the root mean square has a similar meaning as the standard deviation. For a more objective evaluation of the scheme, all statistics should be considered.

Tables 3 and 4 show results obtained by applying the scheme to data from the verifying sample. The scheme was applied every two hours except for a couple of cases where, due to missing radar maps, data 1½ hours apart were used. The reason for adopting a two hour interval is that it results in almost twice the number of cases as compared to the three hour interval. At the same time the two hour intervals still allow us to deal with highly modified rain patterns as opposed to the 30 minute intervals commonly used in the past.

Table 3 is presented in a different format than Table 4 and shows the performance of the scheme for the nonraining days. These days were not included in Table 4 (which shows results from the precipitating days) mainly because of the formulation of the evaluating statistics. When the radar indicates no rain then, $A_R = 0$. If the scheme correctly does not delineate any rain, then $\hat{A}_R = 0$, $R_R = 0$, $R_N = 0$, $N_R = 0$ and $N_N = N$. If the scheme delineates some rain area, then $\hat{A}_R \neq 0$, $R_R = 0$, $R_N \neq 0$, $N_R = 0$ and $N_N \neq 0$. In both cases, most of the evaluating statistics are either undefined or approach infinity. The only statistic which can be used is the percent error.

As can be seen from Table 3 the scheme has correctly predicted no-rain at every time in those two days. For the raining days and according to Table 4

TABLE 3. Performance of the scheme for the nonraining days of the verifying sample.

Time (GMT)	Scheme predicted	Radar indicated	Percent error
	15 May 1984		
1430	no rain	no rain	0.0
1630	no rain	no rain	0.0
1830	no rain	no rain	0.0
2030	no rain	no rain	0.0
	18 May 1984		
1300	no rain	no rain	0.0
1500	no rain	no rain	0.0
1700	no rain	no rain	0.0
1900	no rain	no rain	0.0

[1] One other statistic that is used is the correlation coefficient $\rho_{s,r}$ between the satellite generated rain map and the radar rain map. It is defined as (Lovejoy and Austin, 1979):

$$\rho_{s,r} = (R_R N_N - R_N N_R)/RN.$$

This expression, however is valid only when $A_R = \hat{A}_R$ (i.e., $R_N = N_R$). Such a restriction is not applied to the proposed method; in such a case, the above formula should not be used.

TABLE 4. Error statistics from the raining days of the verifying sample.*

Time (GMT)	POD = R_R/A_R	FAR = $1 - (R_R/\hat{A}_R)$	Percent error f
	21 July 1983		
1730	0.64	0.41	0.24
1930	0.66	0.32	0.16
2130	0.33	0.24	0.11
C**			
	4 July 1983		
2030	0.45	0.26	0.19
2230	0.64	0.21	0.16
C			
	29 July 1983		
1400	0.77	0.29	0.23
1600	0.73	0.20	0.24
1800	0.81	0.42	0.25
2000	0.59	0.58	0.20
2200	0.58	0.70	0.22
N-C			
	13 May 1984		
1530	0.74	0.51	0.31
1730	0.65	0.48	0.24
1900	0.64	0.50	0.29
N-C			
	23 May 1984		
1300	0.81	0.22	0.10
1500	0.78	0.38	0.18
1700	0.65	0.19	0.17
N-C			
1930	0.77	0.35	0.16
2100	0.67	0.32	0.18
C			
Averages	0.66	0.37	0.20

* Areal bias $\beta = 1.11$, error factor $\epsilon_f = 1.33$ and root mean square error $\epsilon_{rms} = 0.29$.
** CC: Convective
N-C: Nonconvective

the proposed scheme results in average values of 0.66 for the POD, of 0.37 for the FAR, of 0.20 for the percent error, and in values of 1.11 for the areal bias, 1.33 for the error factor and of 0.29 for the root mean square error. Figures 8 and 9 are examples of the verification products and performance of the scheme. The above numbers are very comparable with those reported in Lovejoy and Austin (1979). For their midlatitudes warm season data set, and for the area covered by the training radar, their method results in average values of 0.55 for the POD, 0.13 for the percent error and values of 1.13 for the areal bias, 1.26 for the error factor and of 0.22 for the root mean square error. Even though the comparison involves two different data sets, it is apparent that the proposed scheme shows very good skills in delineating rain area. Furthermore, the proposed scheme will delineate the rain areas using the satellite images only, thus not requiring two-dimensional matching with coextensive radar data.

Table 4 (first column) also indicates which cases correspond to convective (C) or to nonconvective (N-C) rain. For the convective cases the average values for POD, FAR, f, β, ϵ_f and ϵ_{rms} are 0.60, 0.30, 0.18, 0.87, 1.36 and 0.28 respectively. For the nonconvective cases the corresponding values are 0.70, 0.40, 0.22, 1.26, 1.31 and 0.30 respectively. The differences are not significant but the convective cases score better with four out of the six statistics. This indicates that the scheme performs better for convective days and suggests that the method could be as successful in the tropics.

As mentioned previously, when a peak which corresponds to raining clouds is located at visible counts less than or equal to 45, then the stability criterion is applied. The 2200 GMT 29 July 1983 case of Table 4 is such a case. The radar map indicated very light, scattered rain. Without the employment of the stability criterion, the scheme delineated a large rain area resulting in a POD of ≈ 0.9 a FAR ≈ 0.8 and a percent error of 0.42. The high value for the POD is only a reflection of the fact that the scheme delineated a large rain area which included the actual small rain areas. With the incorporation of the stability criterion, those numbers have dropped to 0.58 and 0.70 and 0.22 respectively. Even though FAR is still high, the percent error has dropped significantly. This is a good indication of the ability of the employed stability criterion to handle the light rain cases.

An evaluation of the scheme using 3 km CAPPIs instead of radar echo tops resulted in a lower skill score (about 10% lower on the average). The maximum height of the echoes of the precipitation areas over the radar covered area will vary, probably in accordance with the thickness of the clouds. Therefore, the satellite delineated rain area would be best correlated with the echo tops and not with a CAPPI at a specific level.

In addition, it seems that the consideration of an infrared threshold would not improve rain area estimation in the midlatitudes. Of course, for situations described in step 3c, an infrared threshold is a necessity. In all other cases, it is only the peak's visible count that is needed for the rain area estimation. Tests employing infrared thresholds, with or without the peak's visible count, not only did not improve the accuracy of the scheme but resulted in error increases on the average of 15%. Only in two cases (2 May 1983 at 1730 GMT and 4 July 1983 at 2230 GMT) representing severe weather was there an infrared threshold that delineated by itself the rain area as accurately as the peak's visible count. In cases of strong convection, the vertical structure of the clouds may allow a single infrared threshold to delineate accurately the rain area. In the

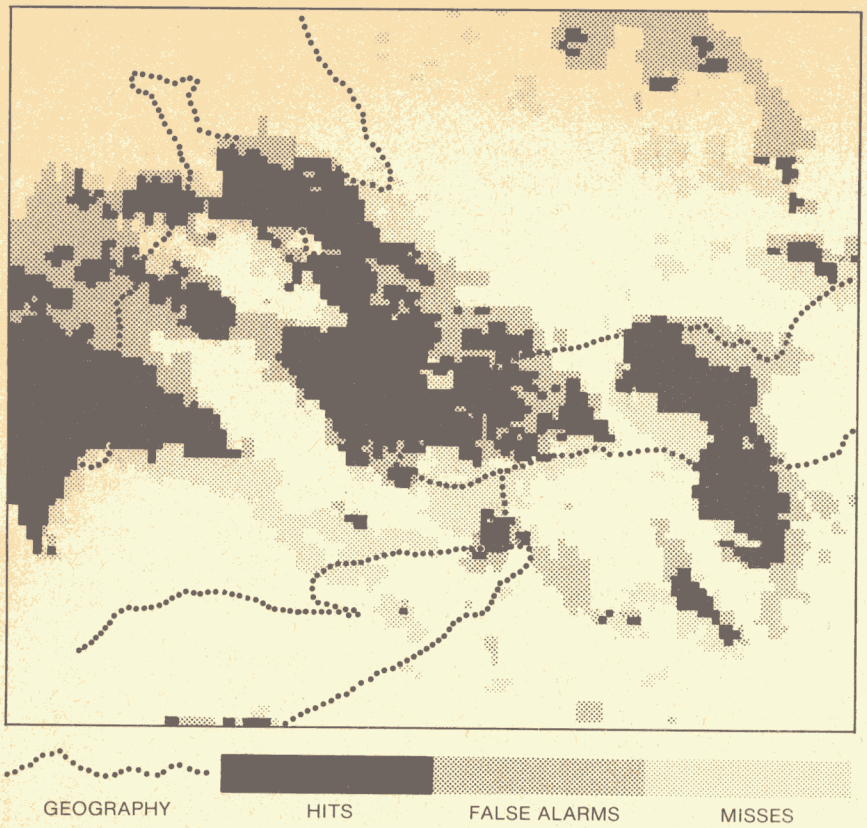

FIG. 8. Example of rain area delineation from the satellite and comparison with the radar for 1730 GMT 21 July 1983. Case of scattered convection.

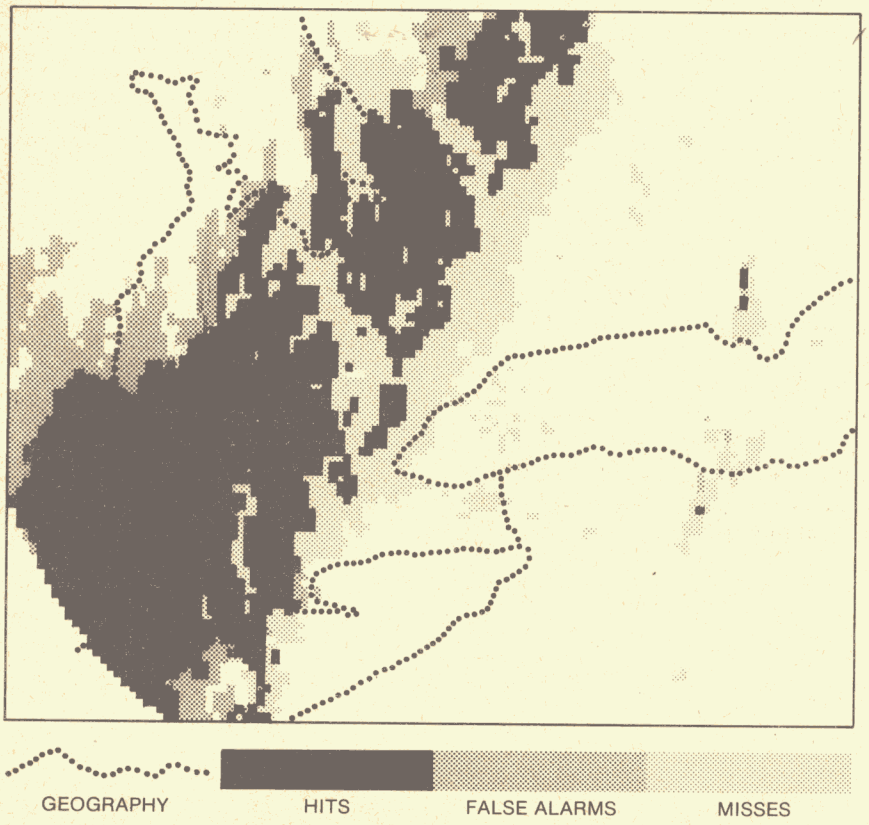

FIG. 9. Example of rain area delineation from the satellite and comparison with the radar for 2230 GMT 4 July 1983. Case of a rain band with embedded strong convective elements.

tropics, therefore, some infrared threshold could be as effective as the peak's visible count.

Infrared data should be considered in the midlatitudes at night, if this method is to be implemented in a real-time operation. The method presented here could also be incorporated with the technique used for classification of the GOES images described in Tsonis (1984b). A new class (rain) could then be defined and separated along with the other classes (clear skies/no snow cover, clear skies/snow cover, high and low broken clouds and overcast).

6. Conclusions

We have presented a new approach for instantaneous rain area delineation in the midlatitudes using GOES visible and infrared data. The method can be described in two parts. In the first part, a technique for the differentiation between raining and nonraining clouds is developed. This technique is based on the location of peaks in the visible/infrared domain. These peaks can be attributed with accuracy to raining and nonraining clouds. In the second part, a scheme which delineates the rain area is presented. The main conclusion is that during daylight the visible image contains more information about rainfall as compared to the infrared image in the midlatitudes. However, in some instances the infrared data are useful in differentiating between raining and nonraining clouds that give similar visible responses. The infrared, apparently, contains as much information as the visible only when strong convection is present. The scheme was found to be very satisfactory in delineating the instantaneous rain area in convective cases, suggesting that the method could also be applied in the tropics. Considering convective and nonconvective cases the resulting average probability of detection was about 66% and the false alarm ratio was about 37%. The main advantage is that the scheme does not require coextensive radar data for the rain area delineation, which makes the method simpler and more flexible than some previously used techniques.

Acknowledgments. Special thanks are extended to the personnel of the Aerospace Division and especially to Mr. E. Morrissey, Mr. D. Steenbergen and Mr. P. King. We would also like to thank Mr. P. Denhoed for helping us with the data processing and Ms. C. Sguigna for typing the manuscript.

REFERENCES

Barrett, E. C., 1970: The estimation of monthly rainfall from satellite data. *Mon. Wea. Rev.*, **98,** 322–327.

——, and D. W. Martin, 1981: *The Use of Satellite Data in Rainfall Monitoring.* Academic Press, 340 pp.

Bellon, A., 1979: The development of a real-time automated system for short-range precipitation forecasting using combined radar and satellite data. Final report to AES (DSS) Contract OSU 78-0056, DSS File 01SU.KM601-8-0253 (available from Stormy Weather Group, McGill University), 92 pp.

——, S. Lovejoy and G. L. Austin, 1980: Combining satellite and radar data for the short range forecasting of precipitation. *Mon. Wea. Rev.*, **108,** 1554–1566.

——, A. Kilambi and G. L. Austin, 1982: Analysis of the navigational error and development of an automated visible normalization procedure and severe weather delineation technique using GOES satellite imagery. McGill Radar Weather Observatory Rep., 78 pp.

Crozier, C. L., and J. W. Scott, 1981: A C-band weather radar system with spherics to serve multiple diverse users in the Canadian climate. *Preprints 20th Conf. on Radar Meteorology,* Boston, Amer. Meteor. Soc., 749–756.

Follansbee, W. A., 1973: Estimation of average daily rainfall from satellite cloud photographs. NOAA Tech. Memo. NESS44, 39 pp.

Griffith, C. G., W. L. Woodley, P. G. Grube, D. W. Martin, J. Stout and D. N. Sikdar, 1978: Rain estimation from geosynchronous satellite imagery—Visible and infrared studies. *Mon. Wea. Rev.*, **106,** 1153–1171.

Gruber, A., 1973: Estimating rainfall in regions of active convection. *J. Appl. Meteor.*, **12,** 110–118.

Lintz, J., Jr., and D. S. Simonett, 1976: *Remote Sensing of Environment.* Adison-Wesley, 694 pp.

Lovejoy, S., and G. L. Austin, 1979: The delineation of rain areas from visible and IR satellite data for GATE and mid-latitudes. *Atmos-Ocean,* **17,** 77–92.

Martin, D. W., and V. E. Suomi, 1972: A satellite study of cloud clusters over the tropical North Atlantic Ocean. *Bull. Amer. Meteor. Soc.*, **53,** 135–156.

Scofield, R. A., and V. J. Oliver, 1977: A scheme for estimating convective rainfall from satellite imagery. NOAA Tech. Memo. NESS 86, 47 pp.

Sikdar, D. N., 1972: ATS-3 observed cloud brightness field related to a meso-to-synoptic scale rainfall pattern. *Tellus,* **24,** 400–413.

Stout, J. E., D. W. Martin and D. N. Sikdar, 1979: Estimating GATE rainfall with geosynchronous satellite images. *Mon. Wea. Rev.*, **107,** 585–598.

Tsonis, A. A., 1984a: Determination and correction of the relative shift between the visible and thermal infrared GOES sensor images. *Int. J. Remote Sensing,* **5,** 975–979.

——, 1984b: On the separability of various classes from the GOES visible and infrared data. *J. Climate Appl. Meteor.*, **23,** 1393–1410.

Woodley, W. L., and B. Sancho, 1971: A first step toward rainfall estimation from satellite cloud photographs. *Weather,* **26,** 279–289.